SOLAR IMPULSE – GROUND VIBRATION TESTING AND FINITE ELEMENT MODEL VALIDATION OF A LIGHTWEIGHT AIRCRAFT

Marc Boeswald[1], Arne Vollan[2], Yves Govers[1], Peter Frei[3]

[1] Deutsches Zentrum für Luft- und Raumfahrt e.V. (DLR)
Institute of Aeroelasticity, Bunsenstr. 10, D-37073 Göttingen, Germany
marc.boeswald@dlr.de

[2] AeroFEM GmbH Simulation and Engineering
Aumuehlenstr. 10, CH-6373 Ennetbürgen, Switzerland
avollan@aerofem.com

[3] Solar Impulse SA
EPFL Scientific Park, Route J.-D. Colladon, CH-1015 Lausanne, Switzerland
peter.frei@solarimpulse.com

Keywords: ground vibration testing, apparent mass, model validation, model updating

Abstract: This paper addresses the challenges in ground vibration testing and in finite element model updating of superlight aircraft structures where the influence of the surrounding air on experimental modal data is no longer negligible. This so called apparent mass effect can lead to complex experimental mode shapes and to biased estimates for experimental damping ratios and experimental eigenfrequencies obtained from ground vibration test. It is essential that the effect of surrounding air on experimental modal data is properly understood to detect finite element model parameters that need to be adjusted while at the same time to avoid adjustment of unreasonable parameters in model updating.

1 INTRODUCTION

"The Solar Impulse project ... aims to have an airplane that can take off and fly autonomously, day and night, propelled uniquely by solar energy, right around the world without fuel or pollution. An unachievable goal without pushing the current technological limits in all fields...". This citation from the Solar Impulse homepage describes the engineering challenges for the aircraft development. The particular design and the use of novel materials made it possible to produce an aircraft with 63 meters wing span and an empty weight of no more than 1.6 tons. This superlight design demands very accurate testing procedures. In addition, the ratio of the apparent mass of the surrounding air to the structural mass is no longer negligible and requires a new approach for the model validation process.
This paper will give insight in a two step model validation strategy. The dynamic characteristics of a) the primary load carrying structure and b) the fully assembled aircraft equipped with solar panels were determined experimentally in two separate ground vibration test (GVT) campaigns. The modal parameters extracted from first GVT campaign were used to update the finite element (FE) model of the load carrying structure at first. Afterwards, the second GVT campaign was used to validate the finite element model of the aircraft ready for flight including control system and electrical systems.
The GVT procedures for testing aircraft with eigenfrequencies considerably below 1 Hz are reviewed and some selected results are presented. For strategy for finite element model updating including the apparent mass effect on eigenfrequencies and mode shapes with is discussed.

2 FUNDAMENTALS OF SOLAR AIRCRAFT DESIGN REQUIREMENTS

Solar Impulse is a true all electric aircraft that is designed for long duration flights or even permanent flights by using solar power as a unique source of energy. It is capable of carrying one pilot around the world without consuming energy based on fossil fuels. Thus, the Solar Impulse project seeks to explore the current possibilities of manned air transportation and to push the limits especially in structural design with new concepts and materials and in development and integration of electrical systems and power management for solar powered aircraft. But how should an aircraft look like that is supposed to fulfil such a challenging mission? To this end, the design criteria such as availability of solar power and power requirements of solar aircraft are briefly reviewed. A more detailed review can be found in reference [1].

The theoretical (extraterrestrial) amount of solar power that is available on our planet is 1367 W/m^2. This is the so called solar constant. Due to absorption in the atmosphere by dust, natural humidity, clouds, etc. the effective amount of solar power is of course less. Furthermore, the geographical latitude position and the angle of incidence of light on solar panels considerably reduce the available amount of solar power. In fact, the maximum value of solar energy that can be harvested at a central European location (e.g. near Munich) is approximately 900 W/m^2 at noon in the summer period. In the winter period, this value is further reduced to not more than 300 W/m^2. Thus, the period of the year has strong influence on availability of solar power. The percentage of daylight hours per day has even more significant impact. Whereas in the summer period in central Europe approximately 900 W/m^2 of solar power is available at the noon peak, the average per day is no more than 260 W/m^2. This value will be reduced even more when taking into account that the efficiency factor of today's solar cells is about 25% for conventional solar cells installed on buildings. The theoretical limit of efficiency for solar cells is about 30%. It is obvious that going from 25% to 30% is strongly correlated with the cost of the solar cells. Taking this into account and also the energy losses in charging and discharging electrical batteries, the total efficiency factor of the propulsion chain of Solar Impulse must be expected to be no more than 12%.

The variation in the availability of solar power during an average day causes a strong requirement for energy storage for permanent (i.e. day and night) operation of solar aircraft. For example, in the daylight period of the day, enough energy must be acquired that can be expended during night to maintain flight altitude. The energy can be stored in two different ways. The most obvious way is electrical power stored in batteries that are charged during the daylight period. The other energy storage is potential energy in terms of flight altitude.

When reviewing the laws of flight physics, it is clear that the power required for constant level flight depends on flight velocity v_∞ (i.e. the free stream velocity) and drag force f_{drag}:

$$P = f_{drag}\, v_\infty \tag{1}$$

The drag force itself is a function of flight velocity, air density ρ (that is a function of flight altitude), area of the wing planform A_{plan}, and the coefficient of drag c_{drag}:

$$f_{drag} = \tfrac{1}{2}\rho v_\infty^2\, c_{drag}\, A_{plan} \tag{2}$$

There is a strong requirement on the minimum flight velocity coming from the minimum lift force to maintain flight altitude. The lift force f_{lift} is a function of air density, flight velocity, coefficient of lift c_{lift}, and area of the wing planform:

$$f_{lift} = \tfrac{1}{2}\rho v_\infty^2 c_{lift} A_{plan} \geq mg \tag{3}$$

The lift force must be equal to the gravity force mg of the aircraft. From this relation, the minimum flight velocity can be deduced:

$$v_\infty \geq \sqrt{\frac{2mg}{\rho c_{lift} A_{plan}}} \tag{4}$$

Inserting equations (4) and (2) into equation (1) yields the power requirement for constant level flight of aircraft:

$$P = \tfrac{1}{2}\rho\, c_{drag} A_{plan} \left(\frac{2mg}{\rho c_{lift} A_{plan}} \right)^{\frac{3}{2}} = \frac{c_{drag}}{c_{lift}} \sqrt{\frac{2(mg)^3}{\rho c_{lift} A_{plan}}} \tag{5}$$

As can be seen, the total mass of the structure m (including the mass of primary structure, electrical systems, solar arrays, payload, and pilot) has strong influence on the power required. For increasing the flight altitude, additional power must be provided that depends on the gravity force and the vertical climb velocity v_{climb}, i.e. the increase of altitude Δh in a certain amount of time Δt:

$$P = \frac{c_{drag}}{c_{lift}} \sqrt{\frac{2(mg)^3}{\rho c_{lift} A_{plan}}} + mg\, v_{climb} = \frac{c_{drag}}{c_{lift}} \sqrt{\frac{2(mg)^3}{\rho c_{lift} A_{plan}}} + mg \frac{\Delta h}{\Delta t} \tag{6}$$

When considering the available power per area of the wing planform, equation (7) applies, where the electrical power P_{ch} required for charging (or discharging) the electrical batteries is also considered. It is obvious that required power per area of the wing planform as stated in equation (7) must be smaller than the average solar power available per day, i.e. in average it must not exceed 260 W/m^2:

$$\frac{P}{A_{plan}} = \frac{c_{drag}}{c_{lift}} \sqrt{\frac{2(mg)^3}{\rho c_{lift} A_{plan}^3}} + \frac{mg}{A_{plan}} \frac{\Delta h}{\Delta t} + \frac{P_{ch}}{A_{plan}} \tag{7}$$

The coefficients of drag and lift are aircraft design parameters that depend on the aerofoil profile selected for the desired cruise speed. The air density is a reciprocal function of the flight altitude but is not a preliminary design parameter. In principle, the area of the wing planform A_{plan} and the total mass of the aircraft m (including pilot, payload, and electrical systems) are the major design parameters that must be optimized. It is known that the total drag force of a wing can be reduced not only by reducing the coefficient of drag, but also by increasing the wing aspect ratio. Thus, a straight wing with high wing span and relatively low chord length is certainly the best choice for Solar Impulse. From a point of view of aeroelasticity, a good balance must be found for the wing aspect ratio to prevent the final wing design from being to flexible.

The parameters Δh and Δt as they appear in equation (7), as well as the battery charging power P_{ch} are optimization parameters that are used to shape the mission profile, i.e. the flight altitude as a function of time of day. A well balance mission profile is required to cope with the variation in the availability of solar power and with the energy storage capabilities in terms of electrical energy (batteries) and potential energy (flight altitude). A feasible mission profile is shown in Figure 1 and is defined as follows: The aircraft already in flight starts collecting solar power at the beginning of the daylight period of the day. At this time, the aircraft will have its minimum flight altitude. The energy collected is used to charge the (relatively empty) batteries but also to increase the flight altitude. At the end of the daylight period, the aircraft shall have its maximum flight altitude and fully charged batteries. During night, the batteries are discharged and the flight level is permanently decreased in order to maintain the flight velocity that is required to generate lift force.

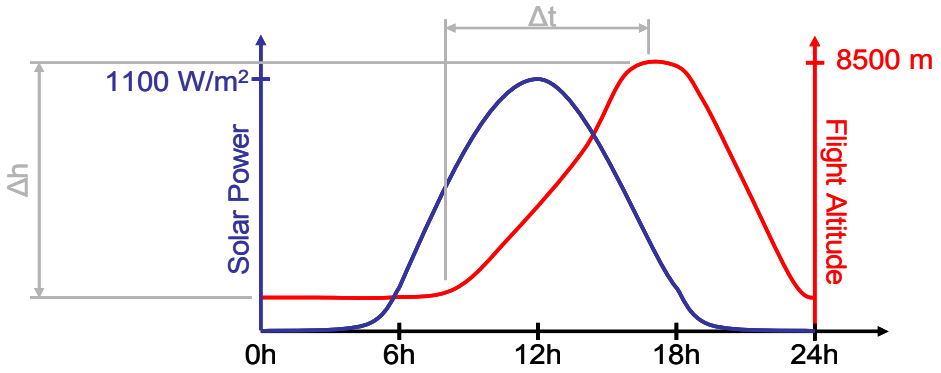

Figure 1: Sketch of a mission profile of Solar Impulse

3 DESCRIPTION OF THE AIRCRAFT

The design of Solar Impulse required several loops of multi-disciplinary optimization with focus on the power requirements reviewed in the previous chapter. Finally, it turned out that for fulfilment of its challenging mission Solar Impulse is required to have approximately 200 m^2 of solar cells for permanent operation day and night. About 180 m^2 with 10748 solar cells are located on the straight wing with 63 m wing span and roughly 3 m chord length. Additional 20 m^2 with 880 solar cells are located on the horizontal tail plane. The aircraft is propelled by 4 electrical engines, each having 7,46 kW. The propellers were specifically designed for a cruise speed of 70 km/h. The batteries that serve as an energy buffer turned out to have a weight of ca. 100 kg per item. They are installed directly behind the propellers and the electrical engines in the engine nacelles. Due to their heavy weight they help to reduce wing bending moments during flight. Figure 2 show the Solar Impulse HB-SIA prototype in flight. The features of this aircraft are summarized in Table 1.

Figure 2: Solar Impulse HB-SIA Prototype

Length:	21.85 m
Wing Span:	63.4 m
Height:	6.4 m
Take Off Speed:	35 km/h
Cruise Speed:	70 km/h
Max. Altitude:	8500 m
Empty Weight:	1600 kg
Seating Capacity:	1
Engines:	4 elec. Eng.

Table 1: Summary of Solar Impulse HB-SIA features

4 GROUND VIBRATION TESTS

A ground vibration test (GVT) is typically carried out on an aircraft structure to experimentally determine the structural dynamics characteristics in terms of modal parameters such as eigenfrequencies, damping ratios, mode shapes and generalized mass. The frequency range considered in a GVT is limited but adapted to the type of structure, to its mission profile, and to the intended usage of the experimental modal data like, for example, the assessment of aeroelastic stability, the verification of a numerical model of the aircraft structure, or the application of structural dynamics modification. The result of a GVT mainly consists of a representative modal model of the aircraft structure that fully describes its structural dynamics in the considered frequency range. That requires properly scaled modes with accurate generalized mass which is highly important for subsequent aeroelastic stability analysis (flutter analysis).

4.1 Test Strategy

In case of the Solar Impulse aircraft, the intended usage of the experimental modal data obtained from the GVT was the verification of the numerical model from the very beginning. The prediction capability of the FE model should be verified based on the assessment of the deviations between simulated modal data and experimental modal data. This includes the

adjustment of specific parameters of the numerical model (i.e. model updating) in case of significant test-analysis deviation.
Due to the lightweight structure, a very detailed FE model was necessary for the stress analysis of the primary structure in the design phase. Consequently, there is a tremendous amount of FE model parameters that need to be validated from the GVT data. On the other hand, there could be a high number of parameters that may need adjustment. However, in FE model generation, there are always structural components that can be modelled with a high level of confidence. This is especially true when the geometry is simple, the load paths are well defined, and the number of substructures and joints are limited. For example, the wing spar box of Solar Impulse is a symmetrical assembly of three individual box beams along the wing span. Each of these box beams can be modelled with relatively good accuracy, provided that the orientation of the carbon fibre layers and their location in the composite is in accordance with the specifications. The parameters of the structural interfaces cannot be modelled with the same level of confidence due to complicated load paths and/or possibly non-linear load path mechanisms due to the design of the joints. The aforementioned also applies to other aircraft components such as the interface between engine nacelles and the wings, the interface of horizontal and vertical tail plane (HTP and VTP) with the fuselage, and the whole drive chain of the control surfaces. When considered as individual components, they can be modelled with good accuracy, but the structural interfaces between the components suffer from modelling uncertainty.
When model updating or respectively model validation is addressed, exactly those interface parameters are the ones considered for adjustment to align the predicted modal parameters of the FE model with the identified modal parameters from the GVT. This already leads to a significant reduction of candidate FE model parameters that are considered for model updating. But even though this approach is reasonable it has an inherent deficiency: Not all FE model parameters that need adjustment are well observed in the test data (i.e. are sensitive w.r.t. the test data), or else wise, not all sensitive FE model parameters need adjustment.
The solution to this problem would require the performance of multiple tests with the requirement that each candidate FE model parameter for model updating is at least highly sensitive to the test data of one of test cases performed. This can be achieved, for example, by testing the same structure in different boundary conditions, or by performing tests on component level, i.e. the different aircraft components are tested individually, and if necessary, dedicated boundary conditions can be used that are similar to the utilization of the respective component in the final aircraft assembly.
In case of Solar Impulse, all the major components underwent static tests to check the stiffness and deformation behaviour under limit loads and ultimate loads. In addition, the individual components have been weighed to identify their basic mass properties. Even though these static tests were originally performed to optimize the weight of the aircraft, they also helped to build up a final assembly FE model from validated component models so that only the interface parameters need proper adjustment from GVT data.
In order to validate the structural model well before entering the GVT and the flight testing it was decided to perform a preliminary GVT only on the primary structure of the aircraft. This so called first assembly GVT was designed to provide a database for correlation with FE model, and further on, for adjustment of the interface stiffness parameters between the aircraft components. In order to guarantee high quality results, the control system of the aircraft was not installed in this preliminary test and only the wing spar boxes of the lifting surfaces were considered. By proceeding this way, undesired effects of apparent mass of the surrounding air were avoided as far as possible and also possibly non-linear effects of the aircraft control system. Such conditions help to improve the quality of the experimental modal analysis results, because the dynamic response of the structure is better in accordance with the basic

assumption of linearity which is a prerequisite of commercial algorithms used for experimental modal analysis.
While the modal parameters of the 1st assembly GVT served to adjust the FE model of the primary structure, there are still FE model parameters in the full aircraft FE model that need validation. This was covered by a second GVT campaign that has been performed on the fully assembled aircraft. That campaign focused of course on the consolidation of the adjusted FE model of the primary structure, now completed with lifting surfaces, solar panels, landing gears etc. This means, the prediction capability of the primary structure FE model was checked with additional (non-structural) mass. In addition, the full aircraft GVT also focused on FE model parameters that could not be validated from the first GVT campaign. For example, the control system of the aircraft can have a strong influence on its aeroelastic stability. Since no control system was installed in the 1st assembly GVT, the validation of the control system must be performed based on the modal data obtained from the final assembly GVT. Excerpts of the results of the two GVT campaigns are presented later on in this paper.

4.2 Test Procedures

The identification of modal parameters of aircraft structures can be a very demanding task due to several reasons. First of all, the duration of a ground vibration test in the very low frequency range, say between 0.5 Hz and 20 Hz, is typically much longer than in the medium frequency range, say between 50 Hz and 2000 Hz. The reason for this lies with the very long vibration periods and the settling times required in the frequency range around 1 Hz. Furthermore, the desired acceleration signals are orders of magnitude smaller while at the same time the displacement amplitudes are immense. In fact, the high displacement amplitudes are a limiting factor for the excitation force levels, because the stroke of modern vibration exciters used in ground vibration testing of aircraft is limited to ±25 mm. Installing the shakers at positions with little displacement amplitudes is not a solution to this problem, because this would in turn have an adverse effect on the accuracy of driving point acceleration measurements and thus on the generalized mass whose quality depends on accurate driving point response measurements. This means, accurate generalized mass requires high vibration amplitudes at the driving points, while at the same time, one is very limited with driving point displacement amplitudes due to exciter stroke limits. This is one of the challenges in testing large aircraft and one has to find a good balance between these two limiting factors.
Accurate identification of generalized mass also requires that the influence of test equipment installed on aircraft is negligible. In case of Solar Impulse it was necessary to install a high number of acceleration sensors on the aircraft to observe its complicated mode shapes. In order to have highly accurate experimental modal data, only the sensors and a few centimetres of the sensor cables were connected to the structure. The majority of the cabling was connected to ropes that were spanned above the aircraft in order to release the aircraft structure from the non-structural mass of the test equipment.
Another point to consider in low frequency testing is noise contamination. At low frequencies, and consequently low acceleration signal levels, the signal-to-noise ratio decreases. This is especially true when cable lengths from sensor to data acquisition system exceeds 100 meters and other work next to the GVT is ongoing in the testing hall. In case of Solar Impulse, dedicated acceleration sensors based on the piezo-resistive measurement principle were used. Due to their specific design, these sensors can measure accelerations down to 0 Hz and can even detect gravity. In addition, amplification of the signal levels has been applied very close to the sensors. Consequently, most of the cable distance between sensor and data acquisition system was covered with a high signal level to effectively reduce noise contamination.

Different test methods have been applied on a complementary basis in the ground vibration test campaign to identify the modal parameters of Solar Impulse. The majority of the mode shapes have been identified using phase separation methods, i.e. experimental modal analysis of frequency response functions (FRFs). Multi-point sweep sine excitation has been used for FRF measurement because of its excellent signal to noise ratio. A data acquisition system with 16-bit analogue to digital (A/D) conversion has been used. Since this is not the latest standard in ground vibration testing, a proper setting of signal ranges prior to A/D conversion was required. This has been achieved by performing very fast preliminary sine sweeps with 3 oct/min and full signal range to assess the maximum signal levels to be expected during the sweep runs for each measurement channel. After such a preliminary sine sweep, the desired sweep runs were performed with the same excitation force level but with much slower sweep rates and with optimized signal ranges derived from the maximum levels occurred in the preliminary sweeps plus a reasonable overhead.
In addition to the phase separation methods, important modes have been measured using the phase resonance method (normal modes tuning), i.e. harmonic excitation using multiple shakers at the same time with appropriated force amplitudes. The phase resonance method has been applied especially for modes that were expected to be non-linear, such as control surface modes, engine modes, etc. The application of the phase resonance method in the very low frequency range is very time consuming but it helps to improve the test data quality (and confidence in the test data) because it yields the experimental modal parameters fully independent from phase separation methods.

4.3 Aircraft Suspension, Boundary Conditions and Rigid Body Modes

Based on preliminary FE analysis, it was anticipated that the lowest elastic mode shapes of the structure would occur significantly below 1 Hz in case of the 1st assembly of the primary structure and around 0.6 Hz in case of the fully assembled aircraft. It is good practice in ground vibration testing to use a soft suspension system as a boundary condition to decouple rigid body modes of the aircraft from the elastic modes. This was no longer possible in case of Solar Impulse, because the decoupling of rigid body modes from the elastic modes would require a suspension system that is extremely flexible. This in turn would yield to displacement amplitudes of the rigid body motion that can easily exceed several meters and this was not compatible with the GVT setup in the test hall.
In general, the approach for validating the FE model does not require to have the aircraft in boundary conditions that are representative for in-flight conditions. Therefore, a dedicated gimbal support (hinge support) was designed that constrained only the vertical rigid body motion. All other (translational and rotational) rigid body degrees of freedom were left unconstrained by linear bearings and journal bearings. It was the intention by using this gimbal device to retain the load paths that typical appear in aircraft vibration modes in order to be able to adjust interface stiffness between aircraft components from the vibration test data. However, boundary conditions always come along with support loads. Since there were only a few points on the Solar Impulse airframe that are qualified to accept the support loads, the gimbal device had to be installed at the main landing gear connection points located on the cockpit structure under the pilot seat. When installing the gimbal device at this position, the mass centre of gravity is located at a higher position than the rotation centre of the gimbal device. Such boundary conditions are known to be unstable. To this end, bungee cords have been installed at several locations on the aircraft and in different directions to stabilize the rigid body modes (i.e. bungees were installed at outer engines vertical, HTP vertical, front fuselage fore-aft, front fuselage lateral). The bungee cords with the desired stiffness specifications were produced on site by coiling up a single rubber fibre of almost infinite

length but with well known elastic properties. By proceeding this way, it was possible to set up well known boundary conditions that were implemented in the FE model for validation purposes.
No attempts have been made to fully identify the modal parameters of all the rigid body modes. Except for the rigid body pitch mode that occurred considerably below 0.4 Hz, all other rigid body modes occurred well below 0.2 Hz. Modal identification at such low frequencies is typically very time consuming. In order to have a rough estimate, the eigenfrequencies of the rigid body modes were identified by counting the vibration periods in a certain time span using manual excitation of a test engineer. It must be stated that due to the friction of the slide bearings in the gimbal device the translational rigid body modes had significant damping. As a consequence, no eigenfrequencies could be identified for the respective translational rigid body modes, because the free vibrations in that modes were over critically damped. Nonetheless, the overall quality of the test setup with the gimbal device and bungees as boundary conditions was excellent. It provided a good decoupling of rigid body modes from elastic modes while retaining the typical vibration behaviour of aircraft. In fact, the eigenfrequency of the first elastic mode shape in the 1st assembly GVT was identified almost a factor of 3 higher than the highest rigid body mode. This is an excellent condition for proper modal identification of the elastic modes. In the full aircraft GVT, the first elastic mode shape was even lower in frequency compared to the 1st assembly test. A reasonable decoupling was still achieved with the gimbal device in this case. This is indicated by a factor of 1.8 between the eigenfrequencies of the highest rigid body mode and the first elastic mode.

4.4 Ground Vibration Test on 1st Assembly

Figure 3 shows the test setup of the 1st assembly GVT that was conducted in December 2008 at the military airport in Dübendorf, Switzerland. The overall dimension of the 1st assembly configuration is about 61 meters wing span, 18 meters length, 6.2 meters height. The mass of this configuration is about 1.4 tons, including 4 dummy masses for the batteries (each ca. 100 kg), four electrical engines with electrical systems and propeller each of about 40 kg, a dummy mass for pilot and electrical systems of 128 kg, and a balancing mass of 195 kg for the gimbal device to shift the mass centre of gravity. The remainder is the mass of the primary structure. It can be seen from Figure 3 that the GVT setup in the low test hall does not allow for excessive rigid body vibrations.

Figure 3: GVT on 1st assembly of the primary structure of Solar Impulse

Even though it was the intention of the 1st assembly GVT that the structure should not be too complex, not less than 76 acceleration sensors were installed to achieve sufficient spatial resolution of the experimental mode shapes. The sensor distribution shown in Figure 4 was well adapted to meet two requirements. First requirement was to distinguish between the FE modes predicted in the frequency range of interest up to 25 Hz in terms of MAC correlation. This implies that the modes of the FE model do not deviate significantly from the true modes of the prototype. Second requirement was to have a good test geometry model that can be used to interpret the test results in terms of animated modes shapes identified in the test.

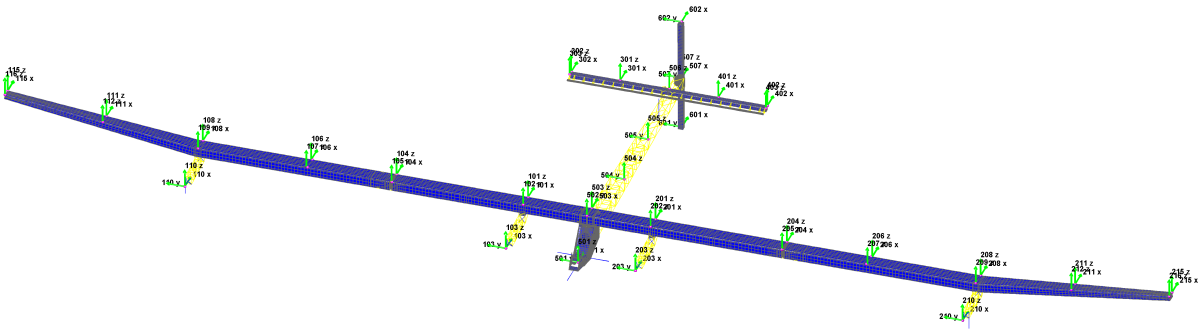

Figure 4: Spatial distribution of sensor locations for 1st assembly GVT

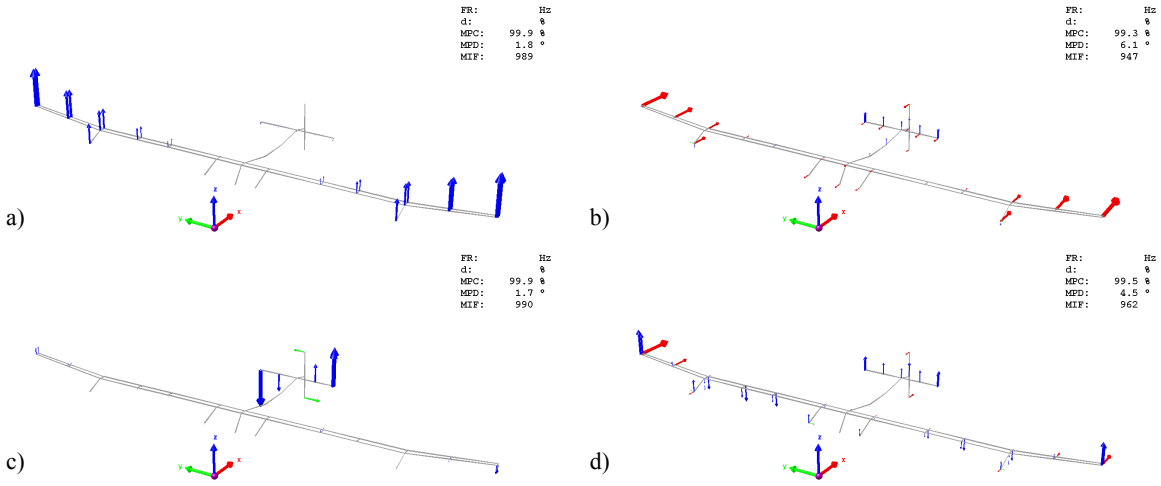

Figure 5: Some fundamental modes of Solar Impulse in 1st assembly configuration
(a: 1st sym. wing bending, b: sym. wing fore-aft, c: fuselage torsion, d: sym. wing torsion)

The essential objective of the 1st assembly GVT was to identify the modal parameter of the basic mode shapes of all structural components, i.e. wing spar box, fuselage, engine nacelles, wing spar box of HTP, wing spar box of VTP for consolidation of the component modelling. In addition, focus has been put to mode shapes that are suitable for the adjustment of structural interfaces stiffness. This requires mode shapes that have significant relative motion of aircraft components, e.g. engine vs. wing, fuselage vs. wing, HTP vs. fuselage, vertical tail plane vs. fuselage, etc. Since the interface stiffness are prone to non-linearity, the majority of these modes were identified on different excitation force levels and using phase resonance method, in particular for the engine nacelle modes.

In addition to the basic modes of the aircraft components, there were quite a few global modes that can be used for adjustment of interface parameters, e.g. engine nacelles vs. wing, fuselage vs. wing, etc. It was concluded from phase resonance tests that most of them had negligible non-linear behaviour.

4.5 Ground Vibration Test on fully assembled Aircraft

The second GVT campaign was performed on the fully assembled Solar Impulse aircraft in January 2010 in Dübendorf, Switzerland. The structural configuration tested is representative for the first flight. The setup is shown in Figure 6. In contrast to the 1st assembly GVT, the wing spar box was assembled with ribs at leading and trailing edges that have a distance of 60 to 80 cm in span wise direction. The solar cells integrated into plastic sheets are connected to these rips so that the upper wing surface has the typical shape of the aerofoil profile required for the desired cruise speed. The lower wing surface is covered with a plastic film. It is clear that the lift forces act on the solar panels. Nonetheless, the solar panels are connected to the ribs of the wing spar box in such a way that they do not add stiffness and will not undergo elastic deformation in case of wing bending. The obvious reason for this is the fragility of the solar cells. The construction of the horizontal tail plane is similar to the wing: Solar cells on upper surface, plastic film on lower surface. The fuselage and the vertical tail plane are fully covered with plastic films.
The overall size of the structure is 63.4 meters wing span, 19.4 meters length (without antennas), and 6.4 meters height. The overall weight of the structure is about 1.7 tons including payload. Concerning the wing span, it has A340 dimensions while the weight is only 1% of the empty weight of an A340.

Figure 6: GVT on fully assembled Solar Impulse

As can be seen from Figure 6, there is significant static deformation due to gravity. The influence of pre-loading due to gravity on the modal parameters has been checked prior to the GVT by eigenvalue analysis of the FE model with and without gravity loads. It was concluded that the geometric stiffness effect was not significant so that a GVT in different statically deformed configuration was not necessary.
The configuration of the ailerons of Solar Impulse is quite complicated. On each side of the wing, 4 ailerons, one spoiler and an airbrake are connected to the trailing edge. This is required for manoeuvrability of such a huge but slow flying aircraft. In order to reduce the control forces for the pilot, each aileron has a tab attached to its trailing edge. The control

system for the elevator and for the rudder have rather conventional design and did not require special consideration. It must be stated, however, that the levers, push-pull rods, etc., i.e. the typical elements of a manual control system of a small aircraft, have extreme lightweight design. Even the ropes for the rudder control are made of carbon fibre.

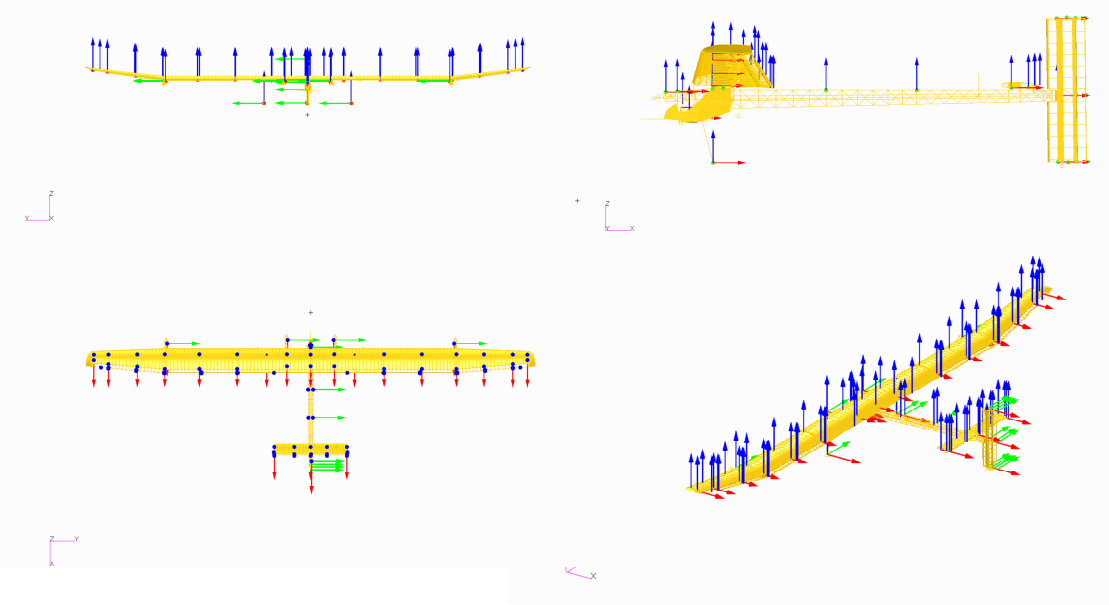

Figure 7: Distribution of acceleration sensors for final GVT on the FE model of Solar Impulse

The boundary conditions of the full aircraft GVT are identical to the 1st assembly GVT. The gimbal device has been re-installed in combination with bungee cords to stabilize the rigid body modes. This time, however, the bungee cords had different stiffness due to different mass and mass centre of gravity of this configuration.

Due to the complexity of the structure, 156 acceleration sensor have been installed. On the wing itself, 84 sensors were required to observe the complicated deformation of wing with ailerons, tabs and spoilers. The frequency range of interest in the second GVT was up to 15 Hz. The sensor distribution used for the full aircraft GVT is shown in Figure 7 on the FE model of the aircraft.

According to FE model predictions, about 90 modes were expected in that frequency range. Since there was no information available about the stiffness of the control system, the frequency range covered in the test was extended up to 20 Hz in order to make sure that one of the major tasks can be achieved, i.e. the identification of all control surface modes for validation of the FE model of the control system.

A typical difficulty is the stiffness of the control system during flight when the pilot is included as a boundary condition. To this end, two extreme cases were investigated. In one case, the control system remained completely free at the pilot seat, whereas in the other case, the control stick was rigidly connected to the cabin. These two cases represent the lower and upper limits for the stiffness of control system.

In total, 72 different modes were identified in the second GVT campaign, plus 6 rigid body modes for which only the eigenfrequencies are available. Figure 8 shows a set of mode shapes that have been identified. These are directly comparable to the modes of the 1st assembly GVT shown in Figure 5. In addition to the airframe modes, the control surface modes are available from two different configurations. This is considered as a rich database available for consolidation of the FE model of the primary structure and for the adjustment of FE model parameters of the control system.

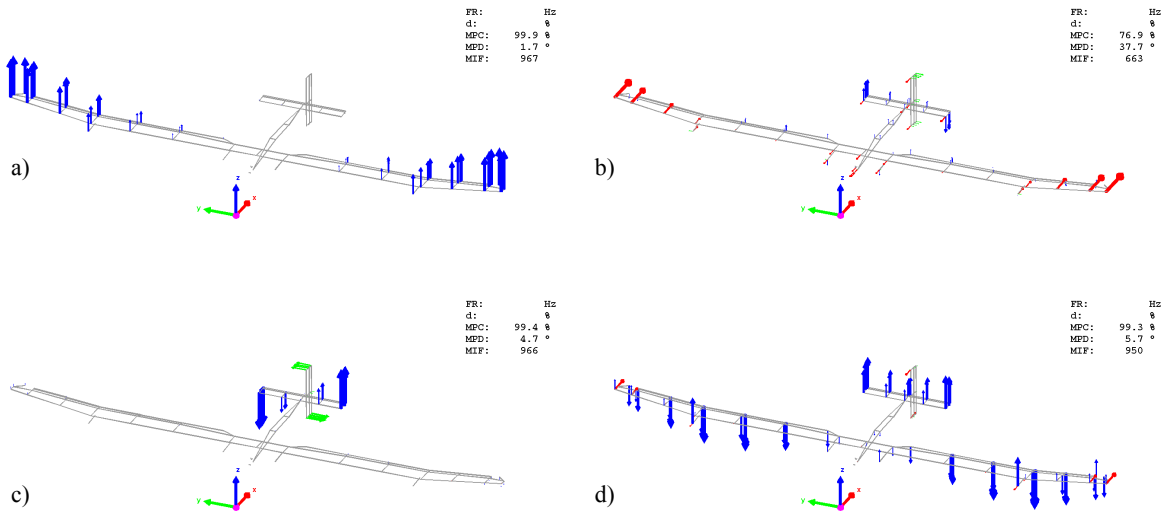

Figure 8: Some fundamental modes of Solar Impulse in final GVT configuration
(a: 1st sym. wing bending, b: sym. wing fore-aft, c: fuselage torsion, d: sym. wing torsion)

5 ANALYTICAL MODEL

Two separate GVTs were performed on two different configurations of Solar Impulse with different assembly levels. According to this, model validation I also performed using this two step strategy. The FE models corresponding to the GVT configurations of Solar Impulse are summarized below. At first, the FE model of the 1st assembly GVT configuration is shown in Figure 9. A summary of the FE model features in terms of grid points, degrees of freedom, element types etc. is given in Table 2. The FE model of the full aircraft GVT configuration is shown in Figure 10 and the corresponding summary is given in Table 3.

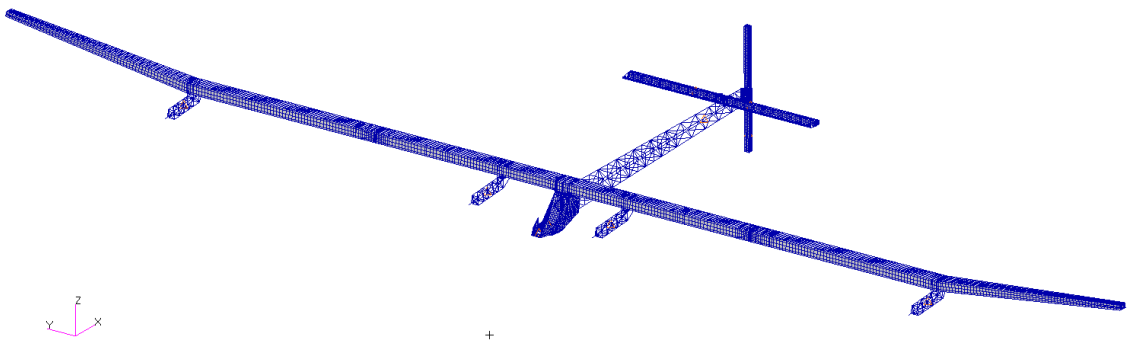

Figure 9: Finite element model of Solar Impulse 1st assembly GVT configuration

Feature	Quantity	Feature	Quantity
GRID	21779	CROD	36
DOF	130674	CBAR	2135
RBE2	63	CBEAM	3772
RBE3	10	CTRIA3	747
PLOTEL	0	CQUAD4	18656
CONM2	11	CHEXA	0
CELAS2	0	CPENTA	0
CDAMP	0		

Table 2: Summary of finite element model of Solar Impulse 1st assembly configuration

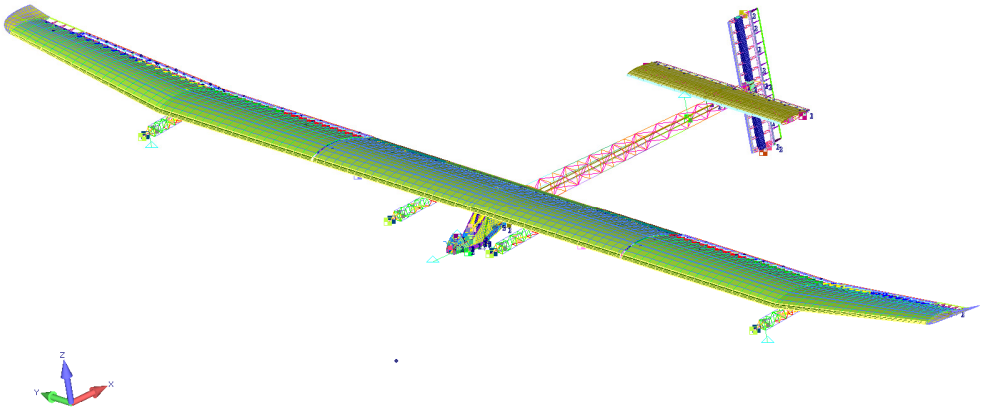

Figure 10: Finite element model of Solar Impulse full assembly GVT configuration

Feature	Quantity	Feature	Quantity
GRID	105276	CROD	48
DOF	631656	CBAR	21718
RBE2	521	CBEAM	5433
RBE3	109	CTRIA3	6377
PLOTEL	648	CQUAD4	92901
CONM2	113	CHEXA	6040
CELAS2	149	CPENTA	1466
CDAMP	4		

Table 3: Summary of finite element model of Solar Impulse full assembly configuration

5.1 Validation Criteria for Finite Element Models

Layout and design of lightweight airframe components takes advantage of numerical simulation of critical load cases such as manoeuvre-, ground-, and gust loads. Such numerical simulations can only yield meaningful results if the numerical models are validated. Model validation for dynamic simulations can be achieved e.g. by minimization of the differences

between experimental and analytical modal data by tuning stiffness and mass parameters of the FE model. This approach to model validation is referred to as FE model updating.
There is no obligatory standard for validation criteria for FE models. This means, the acceptance of FE models for predictive numerical simulations is dependent to a large extent on engineering judgement. In fact, the validation criteria is also dependent on the type of structure, or respectively, on the respective demands for save and reliable operation of the structure. It is not a surprise, for example, that guidelines for model validation are defined in spacecraft engineering, see [2], [3], and [4], where safety factors are small compared to other engineering disciplines. The model validation references cited here represent criteria applied at NASA and US Air Force. Reference [5] provides a summary and interpretation of these model validation criteria. This summary is repeated here in Table 4 for completeness.

Source	$\lvert\Delta f_i\rvert / f_i$	TOR_{ii}	$\lvert TOR_{ij}\rvert$	XOR_{ii}	$\lvert XOR_{ij}\rvert$
NASA 1991	$\leq 5\%$	1.0	< 0.1	> 0.9	< 0.2
NASA 1996	$\leq 5\%$	1.0	< 0.1	> 0.9	< 0.1
USAF 1999	$\leq 3\%$	1.0	< 0.1	> 0.95	< 0.1

Table 4: Model validation criteria of three different spacecraft engineering guidelines

The percentage of eigenfrequency deviation is denoted here as $\lvert\Delta f_i\rvert / f_i$. It may represent the deviations of the eigenfrequency of a test mode shape from test (superscript *exp*) and the corresponding analytical mode shape of a numerical model (superscript *ana*):

$$\lvert\Delta f_i\rvert / f_i = \frac{\left| f_i^{ana} - f_i^{exp} \right|}{f_i^{exp}} \tag{8}$$

TOR is the so-called "test-orthogonality" that is an indicator for the orthogonality of mode shapes with respect to an analytical mass matrix:

$$\left| TOR_{ij} \right| = \left| \left\{ \phi_i^{exp} \right\}^T \left[M^{ana} \right] \left\{ \phi_j^{exp} \right\} \right| \tag{9}$$

The TOR criterion is to be applied only to the set of experimental mode shapes to verify the quality of the experimental mode shapes prior to their usage in the model validation process.
It should be noted here, that the experimental mode shapes $\left\{ \phi_i^{exp} \right\}$ are assumed to be available as real normal modes and are scaled in such a way that the scalar product of equation (9) is equal to one if $i=j$, i.e. unity generalized mass of the test modes with the analytical mass matrix. This results in TOR_{ii} values that are always equal to *1.0*. TOR_{ij} denotes "cross-orthogonality" between two different test mode shapes i and j. A reasonable approach to transform complex experimental mode shapes into real normal modes is presented in reference [6].
XOR denotes the "cross-orthogonality" between experimental and analytical mode shapes with respect to an analytical mass matrix:

$$\left| XOR_{ij} \right| = \left| \left\{ \phi_i^{exp} \right\}^T \left[M^{ana} \right] \left\{ \phi_j^{ana} \right\} \right| \tag{10}$$

As with the test mode shapes, it is assumed here that the analytical mode shapes are real normal modes that are scaled to unity (analytical) generalized mass.
The aforementioned validation criteria are applied at first to the test mode shapes to the quality of the test data. Those test mode shapes which pass this quality criterion can be used afterwards for cross-orthogonality check with analytical mode shapes of the FE model. It can be seen from Table 4 that the *TOR* criterion applied to the test mode shapes is relatively strong whereas the *XOR* criterion is more relaxed. A model is considered as validated if the test mode shapes that pass the *TOR* criteria and that lie within the frequency range of interest have *XOR* criteria and frequency deviations with corresponding analytical mode shapes corresponding to the criteria mentioned in Table 4. These criteria are slightly different in the references cited here.
The application of the above mentioned cross-orthogonality checks requires mode shapes scaled to unity (analytical) modal mass. The equations (11) and (12) represent the same criterion that can be applied to arbitrarily scaled mode shapes. The similarity to the modal assurance criterion (MAC) can be observed. In order to arrive at the same numerical values as with in the original equations (9) and (10) quadratic scalar products appear in the denominator of equations (11) and (12) and the square root must be applied:

$$\left|TOR_{ij}\right| = \sqrt{\frac{\left(\left\{\phi_i^{exp}\right\}^T \left[M^{ana}\right] \left\{\phi_j^{exp}\right\}\right)^2}{\left(\left\{\phi_i^{exp}\right\}^T \left[M^{ana}\right] \left\{\phi_i^{exp}\right\}\right)\left(\left\{\phi_j^{exp}\right\}^T \left[M^{ana}\right] \left\{\phi_j^{exp}\right\}\right)}} \tag{11}$$

$$\left|XOR_{ij}\right| = \sqrt{\frac{\left(\left\{\phi_i^{exp}\right\}^T \left[M^{ana}\right] \left\{\phi_j^{ana}\right\}\right)^2}{\left(\left\{\phi_i^{exp}\right\}^T \left[M^{ana}\right] \left\{\phi_i^{exp}\right\}\right)\left(\left\{\phi_j^{ana}\right\}^T \left[M^{ana}\right] \left\{\phi_j^{ana}\right\}\right)}} \tag{12}$$

Validation procedures based on the aforementioned criteria have some major disadvantages. At first, it is not taken into account that the test mode shapes may be available as complex modes, or respectively, test data degradation by transforming complex eigenvectors into real normal modes. Secondly, the quality check of the test mode shapes requires an analytical mass matrix. It is common practice to derived this analytical mass matrix from the FE model e.g. by static condensation (Guyan reduction) to the test degrees of freed. There is no indication about the accuracy of this analytical mass matrix, especially in such cases where the distribution of test degrees of freedom is not good for static condensation. At last, the unit systems used for the FE model and the test data can be incompatible. The measurement points can have different coordinates than the nodes of the FE model and the engineering units of generalized mass of test data and analytical data can be different.

5.2 Analytical Modal Data and Consideration of Apparent Mass

The structure of the Solar Impulse aircraft has extreme lightweight design whereas the dimensions are those of a typical transport aircraft. When considering vibrations of such a lightweight structure, the ratio of the structural mass and the mass of the surrounding air that is vibrating along with the structure is no longer negligible. This effect is called the apparent mass effect.
It was discovered that in case of Solar Impulse the eigenfrequency of fundamental wing bending modes deviated from the experimental eigenfrequency considerably more than 15%. The difficulty now is that this deviation can either be caused by erroneous FE model

parameters, or when assuming that all FE model parameters are nominally correct, it can also be caused by the apparent mass effect. It is necessary for FE model updating that the boundary conditions of the test must be applied to the FE model as far as possible. Here, it is also required to take into account the effect of the surrounding air as a boundary condition.
Using the so-called non-structural mass in NASTRAN to model this effect is not a solution, because the vertical symmetric wing bending mode will suffer more from the apparent mass than the fundamental fore/aft bending of the wing. The approach to include the apparent mass effect chosen here was to perform an aeroelastic analysis (i.e. flutter analysis or SOL 145 in NASTRAN). This is a coupled analysis of a structure model with a suitable aerodynamic model that is essentially performed in the modal domain. The structural dynamics part is represented by a modal model of the aircraft and is enhanced with an aerodynamic panel model based on the Doublet Lattice Method (DLM). The flutter equation (13) is a modal equation of motion coupled by aerodynamic forces represented by the dynamic pressure $\frac{1}{2}\rho v_\infty^2$ and the generalized aerodynamic force matrix $[Q]$. This matrix is a function of the Mach number Ma (speed of sound dependent on flight velocity and flight altitude), and the reduced frequency ω_{red}:

$$\left(-\Omega^2[m]+j\Omega[d]+[k]+\tfrac{1}{2}\rho v_\infty^2[Q(Ma,\omega_{red})]\right)\{\hat{q}\}=\{0\} \tag{13}$$

The dimensionless reduced frequency depends on the eigenfrequencies ω_r, the flight velocity v_∞, and on the chord length b of the aerofoil profile:

$$\omega_{red}=\frac{\omega_r b}{v_\infty} \tag{14}$$

For more details on the generation of aeroelastic models in NASTRAN refer to reference [7] or for more general information on aeroelastic analysis to reference [8].
In aeroelastic stability analysis, the flutter equation (13) is solved at different combinations of flight velocity and flight altitude (i.e. at different air densities ρ). Essentially, an eigenvalue problem is solved that yields a new set of complex eigenvalues and complex mode shapes that include the influence of aerodynamic stiffness, damping, and mass. In case of Solar Impulse, the flutter equation was solved using the local altitude level at Dübendorf airport (i.e. approx. 1500 ft) for very low flight velocity approaching zero (i.e. $v_\infty \approx 2 m/s$) in order to obtain mode shapes that include the effect of aerodynamic mass and damping while the aerodynamic stiffness is kept at a minimum.
The results of the flutter analysis (i.e. complex mode shapes and eigenvalues) obtained under these conditions were used afterwards for comparison with test data. An excerpt of the qualitative influence of apparent mass on the eigenfrequencies of different mode shapes is shown in Figure 11. Eigenfrequency deviations and MAC values between results of the FE model and the aeroelastic model is shown there for selected modes in the full aircraft GVT configuration. It should be noted that the absolute numbers of deviation between FE and aeroelastic model cannot be presented here for confidentiality reasons.

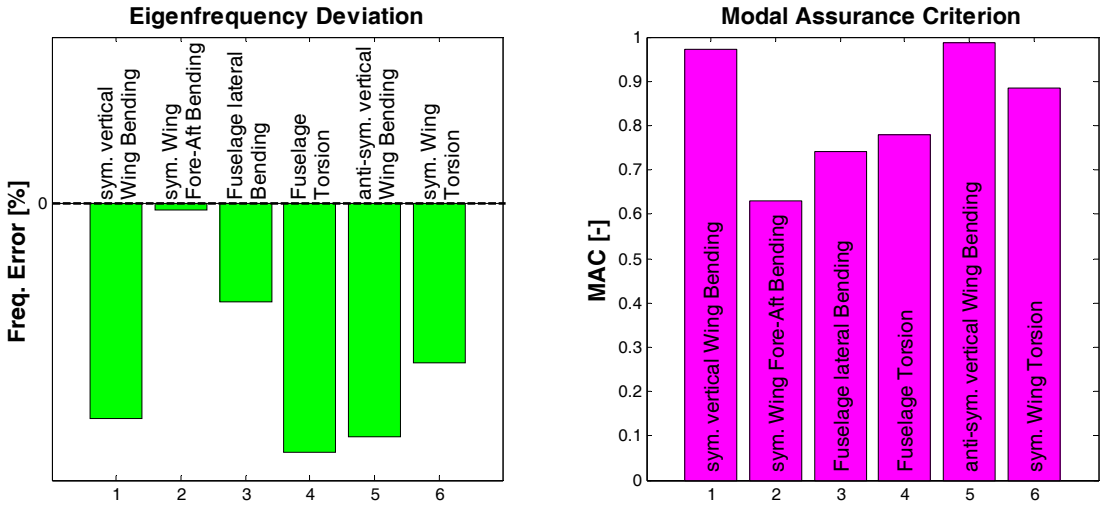

Figure 11: Qualitative influence of apparent mass on eigenfrequencies (FE is reference)

As can be seen, the all eigenfrequencies obtained with the aeroelastic model are lower than the corresponding FE eigenfrequencies. This is in accordance with engineering judgement, because the essential effect of surrounding air is adding mass to the structure. It can also be observed that the influence on the wing fore-aft bending is not as strong as on the vertical bending modes of the structure. The reason for this is the aerodynamic forces that are more effective in a direction normal to the wing planform. It is also interesting to see that the fuselage modes are also affected by apparent mass. The wing bending and wing torsion modes are shown in Figure 12 and it can be seen that the very light tail planes have considerable modal displacement in this case so that it must be expected that these modes suffer a lot from apparent mass effects. In case of the fuselage lateral bending (Figure 12a), the horizontal tail plane is moving more or less in plane which results in lower apparent mass effects. In case of fuselage torsion mode (Figure 12b), both the horizontal and vertical tail planes have modal displacements in directions normal to their wing planforms. Accordingly, the fuselage torsion mode is strongly affected by apparent mass.

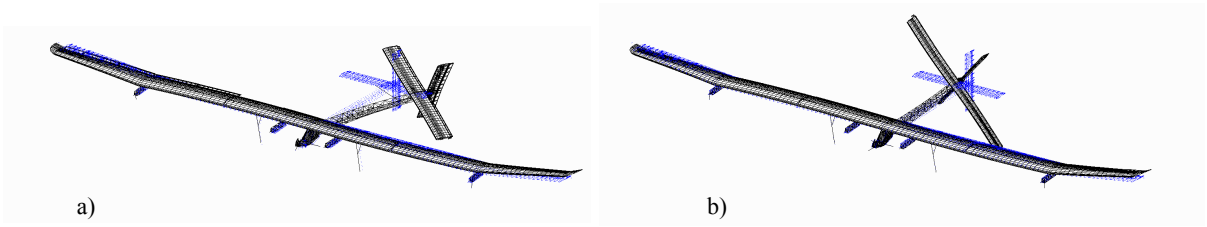

Figure 12: Fuselage lateral bending mode (a) and fuselage torsion mode (b) of the FE model

It should be pointed out that complex modes and eigenvalues are the result of the NASTRAN aeroelastic analysis. Only the real parts of the complex modes were used for correlation with test data because the model validation software requires real normal modes as an input for analytical data. This could be an explanation for the relatively low MAC values between FE modes and modes of the aeroelastic model.

Even though the usage of complex modes from aeroelastic analysis takes into account the apparent mass effects, it brings up further difficulties. For example, the total mass matrix, i.e. structural mass plus apparent mass (aerodynamic mass) is not available as a matrix in physical degrees of freedom but only as a matrix in the modal domain. This makes it impossible to apply the model validation standards discussed in chapter 5.1.

5.3 Model Validation

The approach for model validation takes full benefit of the two-step procedure applied for the GVTs. At first, the stiffness parameters of structural interfaces were updated using the FE model of the 1st assembly GVT configuration and the corresponding experimental data. After this first part of model validation, this FE model was enhanced with ribs, solar cells, control system, etc., to represent the full aircraft configuration. The apparent mass effect was included by using the complex modes and eigenvalues of the aeroelastic model (i.e. coupled FE model and DLM aerodynamic model). The prediction capability of this aeroelastic model was then checked using the GVT data of the full aircraft configuration. The FE model parameters of the control system were updated using the eigenfrequencies of the control surface modes.
An excerpt of the results of model validation is presented in Figure 13. The results are presented for the same modes as summarized in Figure 11. It can be seen that the eigenfrequency deviations of the aeroelastic model (DLM in Figure 13) w.r.t. the GVT data is in most cases lower than the eigenfrequency deviations of the FE model. This indicates the importance of taking into account the apparent mass effect. When using the results of the FE model alone one may come to the conclusion that FE modes number 1, 4, 5, and 6 in Figure 13 deviate significantly from the test data (see the green coloured bars in Figure 13). However, when the same model with the apparent mass effect is used, it becomes obvious that mode number 3 is the one that deviates from the test data (see the blue coloured bars in Figure 13). It is obvious that including the apparent mass effect (or respectively using the aeroelastic model in stead of the FE model) is important to understand which modes really deviate from test data and thus to figure out which FE model parameters need to be updated.
When looking at the results of model validation, however, it must be stated that the correlation of the fuselage lateral bending mode is still not satisfying (i.e. mode number 3 in Figure 13). It is still acceptable, because that mode is not critical demonstration of safe operation of the aircraft within the flight envelope. It was also difficult to achieve a good MAC correlation of the wing fore-aft bending mode (i.e. mode number 2 in Figure 13). It must be stated that the corresponding experimental mode shape is highly complex due to the significant amount of friction damping introduced at the linear bearings of the gimbal device. This local damping mechanism is not contained in the FE model and also not in the aeroelastic model and yields to poor MAC values in both cases.

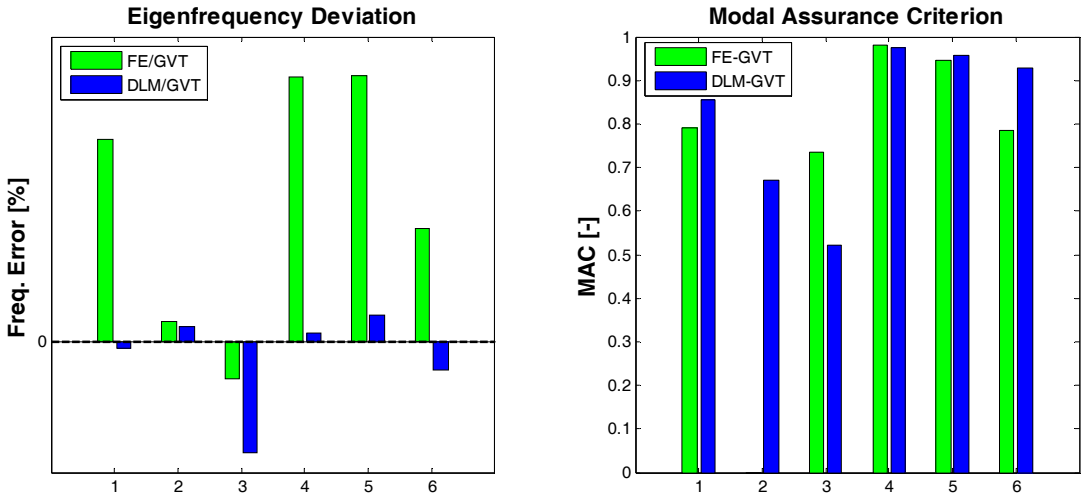

Figure 13: Excerpt from model validation of full aircraft GVT configuration

6 CONCLUDING REMARKS

After reviewing the very basic aspects of preliminary design of solar aircraft, a summary was given about the model validation strategy and the corresponding GVT campaigns performed on the Solar Impulse aircraft for the achievement of the permit to fly. Difficulties with accurate response measurements and vibration excitation in ground vibration testing of lightweight structures at very low frequencies were discussed. A two-step test strategy was adopted to provide rich databases for model validation and excerpts from the GVT results were presented. The extreme lightweight design of the Solar Impulse structure required special consideration of the apparent mass effect in the analytical model. This was achieved by employing aeroelastic analysis using a DLM approach for the aerodynamic forces. Correlation between results of the FE and the aeroelastic model showed the importance of taking into account apparent mass effects to figure out FE model parameters for model updating. Model validation standards have been reviewed but could not be applied in this special case, because a physical mass matrix that includes apparent mass effects is not available from the aeroelastic analysis. The success of the chosen model validation approach was presented and the effect of apparent mass was discussed by comparing GVT data with both, FE model results and results of an aeroelastic model.

7 ACKNOWLEDGEMENTS

The authors from DLR gratefully acknowledge the valuable support of Mr. Marcus Basien (Lead Engineer), and Mr. Frederick Tischhauser (Test Engineer). They contributed to the planning and the performance of the ground vibration test campaign and made sure that everything went smoothly. Furthermore, we want to thank Mr. Arne Vollan from AeroFEM who was responsible for setting up the finite element model and the aeroelastic model. His profound experience in aeroelasticity and NASTRAN is gratefully acknowledged.

8 REFERENCES

[1] ROSS H., *Solarangetriebene Flugzeuge = The True All Electric Aircraft – Eine Übersicht*, DGLR Deutscher Luft- und Raumfahrtkongress 2007, First CEAS European Air and Space Conference, Berlin, September 2007

[2] MSFC-HDBK-1974, *Guidelines for load analyses and dynamic model verification of shuttle cargo elements*, George C. Marshall Space Flight Center, MSFC, AL 1991

[3] NASA-STD-5002, *Load analyses of spacecraft and payload*, NASA Technical Standard, 1996

[4] DOD HANDBOOK-304A (USAF), *Test requirements for launch, upper-stage, and space vehicles, Volume II: Application guidelines*, US Air Force, 1999

[5] HASSELMAN T., LLOYD G., *A top-down approach to calibration, validation, uncertainty quantification and predictive accuracy assessment*, Computer methods in applied mechanics and engineering, Vol. 197, pp. 2596-2606, 2008

[6] FUELLEKRUG U., *Computation of real normal modes from complex eigenvectors*, Mechanical Systems and Signal Processing, Vol. 22, pp. 57-65, 2008

[7] RODDEN W. P., JOHNSON E. H., *MSC.Nastran Version 68 – Aeroelastic Analysis User's Guide*, MSC Software Corporation, 1994

[8] BISPLINGHOFF R.L., ASHLEY H., HALFMAN R.L., *Aeroelasticity*, Dover Publications, 1996